Nuclear Inst. and Methods in Physics Research, A 927 (2019) 287–292

Contents lists available at ScienceDirect

Nuclear Inst. and Methods in Physics Research, A

journal homepage: www.elsevier.com/locate/nima

First experimental demonstration of time-resolved X-ray measurements with next-generation fast-timing MCP-PMT

Junqi Xie [a,*], Robert Wagner [a], Marcel Demarteau [a], Lei Xia [a], Bernhard Adams [b], Zhehui Wang [c], Xuan Li [c], Renyuan Zhu [d], Liyuan Zhang [d], Chen Hu [d], John Katsoudas [e], Yujia Ding [e], Yanhua Shih [f], Thomas A. Smith [f], and the UMA collaboration

[a] Argonne National Laboratory, Lemont, IL 60439, USA
[b] Incom, Inc., Charlton, MA 01507, USA
[c] Los Alamos National Laboratory, Los Alamos,, NM 87545, USA
[d] California Institute of Technology, Pasadena, CA 91125, USA
[e] Illinois Institute of Technology, Chicago, IL 60616, USA
[f] University of Maryland, Baltimore County, Baltimore, MD 21250, USA

ARTICLE INFO

Keywords:
Ultrafast scintillator crystal and detector
Hard X-ray imaging
Microchannel plate photomultiplier
Rise time
Decay time

ABSTRACT

We report the first successful time-resolved X-ray measurements at the APS 10-ID-B beamline by coupling ultrafast scintillators with photodetectors. Multiple scintillator and sensor pairs (LYSO, plastic scintillator, dynode PMTs, MCP-PMT), as well as a standalone detector (diamond), were tested to demonstrate the time-resolved measurements using hard X-rays at energies of 20 keV and above. The experimental results show that a number of choices exist for time-resolved high-energy X-ray beam measurement. Notably, by gating the photocathode, the Argonne fabricated fast-timing microchannel plate photomultiplier and LYSO crystal pair achieved fast signal detection with a rise time of ~6 ns and a decay time of ~33 ns. These experiments pave the way towards ultrafast imaging technologies using hard X-rays for many applications.

Contents

1. Introduction

High-speed X-ray imaging is one of the most important techniques and sometimes the only option for materials studies at micro- and nanosecond timescales [1–3]. Synchrotrons such as the Advanced Photon Source (APS), as the brightest hard X-ray sources today, are uniquely suited to study mesoscopic materials in-operando because of the penetrating power of hard X-rays at energies above 20 keV. Time-resolved experimental data from these and other facilities are essential for predictive model development and validation of computer codes, new materials discovery and applications [4–6]. In-situ measurements also provide a platform to develop new methods of fabrication such as additive manufacturing [7,8]. Higher imaging frame rate requires a

* Corresponding author.
E-mail address: jxie@anl.gov (J. Xie).

https://doi.org/10.1016/j.nima.2019.02.057
Received 15 November 2018; Received in revised form 15 February 2019; Accepted 20 February 2019
Available online 25 February 2019
0168-9002/

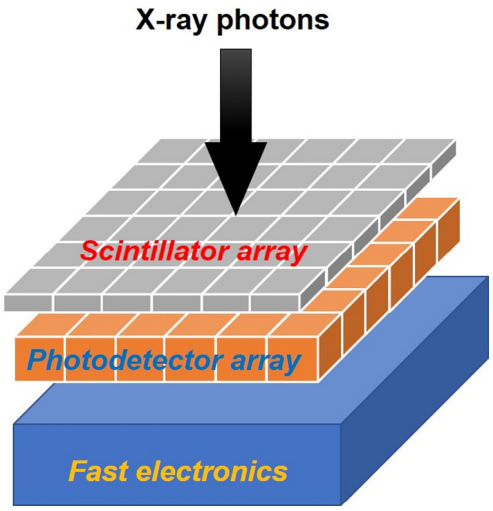

Fig. 1. The schematic concept of an indirect total absorption imager consisting of a pixelated ultrafast inorganic scintillator screen, a pixelated ultrafast photodetector, and ultrafast electronics (Dimension not to scale).

higher X-ray pulse repetition rate. APS Upgrade (APS-U), with 88 MHz pulse repetition with a low beam emittance and more than 10^5 X-ray photons per pulse, is anticipated in the near future [9]. Similar capability is available at the French European Synchrotron Radiation Facility (ESRF) and elsewhere. To take advantages of these new source capabilities and future facilities such as Matter–Radiation Interactions in Extremes (MaRIE) [10], ultrafast hard X-ray imaging capabilities with a frame-rate no less than 100 MHz is desired, which will be at least 10 times faster than the state-of-the-art technologies [11–13].

Innovative ideas and capabilities were proposed to address the requirement and prototype demonstration of ultrafast imaging detector driven by the rapid development of X-ray free electron laser (XFEL) technology [14]. These include the semiconductor sensors for direct detection as well as ultrafast inorganic scintillators and photodetector pair for indirect detection. Fig. 1 shows a schematic concept of an indirect total absorption imager consisting of a pixelated ultrafast inorganic scintillator screen, a pixelated ultrafast photodetector, and ultrafast electronics. The past few years have witnessed the significant progress on the ultrafast scintillators, and multiple scintillators have been identified as possible solutions for an ultrafast front image for gigahertz hard X-ray imaging. For example, the ZnO:Ga crystal, developed as a Wannier excitation-based scintillator, shows sub-nanosecond decay time (< 1 ns) and moderate light yield of 2000 ph/MeV [15,16], the BaF_2:Y crystal based on the core–valence transition holds the record fastest rise time of 0.2 ns and decay time of 0.6 ns [13,17] with suppressed slow component as well as excellent light yield of 2000 ph/MeV. Such fast rise and decay time scintillators call for the ultrafast and efficient photodetectors for light detection. Traditional dynode photomultipliers can only handle signals with a rise time of several nanoseconds [18], microchannel plate-based photodetectors with picosecond time detection capability [19] become one of the most promising candidates for ultrafast signal detection.

Recently, a new generation of fast-timing microchannel plate photomultiplier (MCP-PMT) was developed and commercialized by the LAPPD collaboration [20]. The detector exhibits excellent timing resolution of < 50 ps [21], and rise time of ~0.5 ns [22], suitable for the ultrafast signal detection. Moreover, the detector employs next-generation MCP, which is functionalized by atomic layer deposition (ALD) coating of resistive and secondary emission layers on hollow, 25 μm sized capillary arrays. The ALD technique provides high secondary emission of these MCPs, resulting in MCP-PMT with extraordinary gain level > 10^7 [23], providing excellent single photon detection

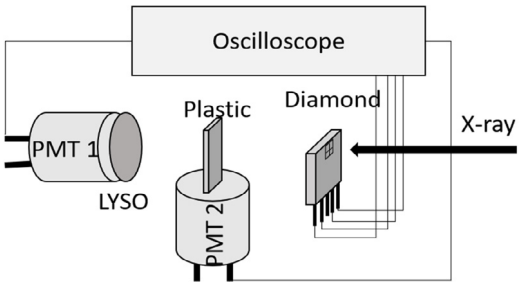

Fig. 2. Proof of concept experiment setup using a sequential set of fast detectors for X-rays at 29.2 keV (Sn K-edge) from APS 10-ID-B. The locations of the detector with respect to the incoming X-rays direction are diamond (4-pixel prototype), plastic scintillator, and high-Z crystal LYSO.

capability and possible high dynamic range. Optimization of the new MCP-PMT towards time-resolved X-ray detector requirement may provide a solution for ultrafast X-ray imaging with fast time response and excellent dynamic range when coupled with ultrafast crystals.

In this paper, we report the first successful time-resolved X-ray measurements at the Advanced Photon Source (APS) beamline 10-ID-B by coupling ultrafast crystals with photodetectors. Multiple scintillator and sensor pairs as well as a standalone detector were tested to demonstrate the time-resolved measurements using hard X-rays at energies of 20 KeV and above. The experiment setup is described in details in this paper, the results are presented and discussed, and the directions on further optimization of the next-generation MCP-PMT design for GHz hard X-ray imaging is also addressed at the end.

2. Experimental samples and methods

The experiment was performed at the APS 10-ID undulator beamline capable of a broad working energy range between 4.5 keV (Ti edge) and 45 keV (Nd k-edge) [24]. The experiment was performed in two beamline time periods: (1) proof of concept experiment with well-known detectors during the standard 24-bunch mode of APS operation; (2) exploration experiment with a coupled scintillator and Argonne fast-timing MCP-PMT during the hybrid fill mode of APS operation.

Fig. 2 shows the schematic of the proof of concept experiment setup. Several detectors were used in series to demonstrate time-resolved hard X-ray measurement, including a diamond quadrant detector, an organic plastic scintillator coupled with a photomultiplier, and an inorganic high-Z Lutetium–yttrium oxyorthosilicate (LYSO) crystal coupled with a photomultiplier. The active area of the diamond detector is 4.7 mm × 4.7 mm and is separated into four quadrants with one analog channel for each quadrant [25]. The plastic scintillator and LYSO crystal are relatively large, and their scintillation lights were read out from a single anode Hamamatsu R2059 photomultiplier, respectively. The individual detectors were first mounted on a breadboard and aligned to the same height. Cosmic ray signal was used prior to the X-ray beam experiments for commissioning purpose. In the validation experiment, the scintillator samples were directly coupled to photodetectors and wrapped with black rubberized fabric. The entire setup on the breadboard was further covered with black fabric to ensure light tightness.

Fig. 3 shows the schematic of the next-generation MCP-PMT used in this experiment. It consists of a bialkali (K-Cs-Sb) photocathode, two ALD functionalized MCPs in chevron configuration and electronics readout. These components are sealed in a vacuum glass envelope for electron multiplication. While the photons generated by scintillator reach the MCP-PMT, the photocathode converts the photons into electrons through photoelectric effect. These electrons enter the HV biased MCP pores and generate secondary electron emission by bombarding the inside wall of the MCP. Electron showers generated by the multiple secondary electron emission processes are collected at the end for signal

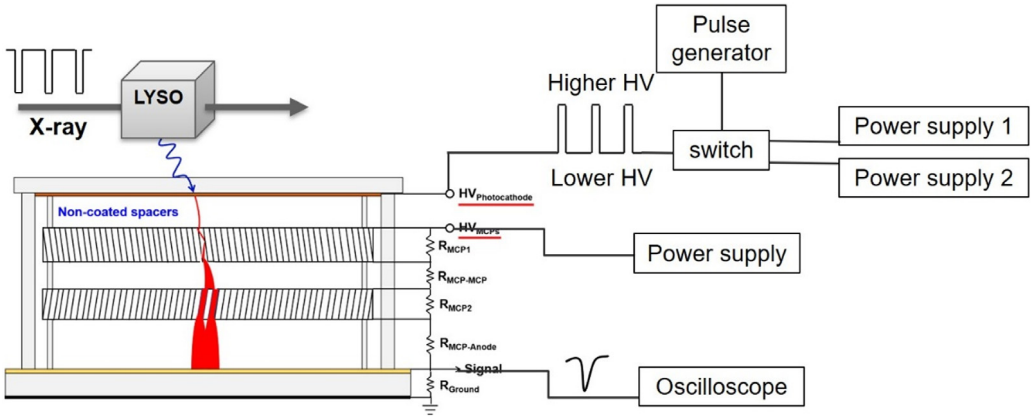

Fig. 3. Schematic of MCP-based photodetector assembly (not to scale) and the electrical circuit diagram during time-resolved X-ray measurement using coupled MCP-PMT and LYSO. The photocathode is gated by the pulse generator and two power supplies.

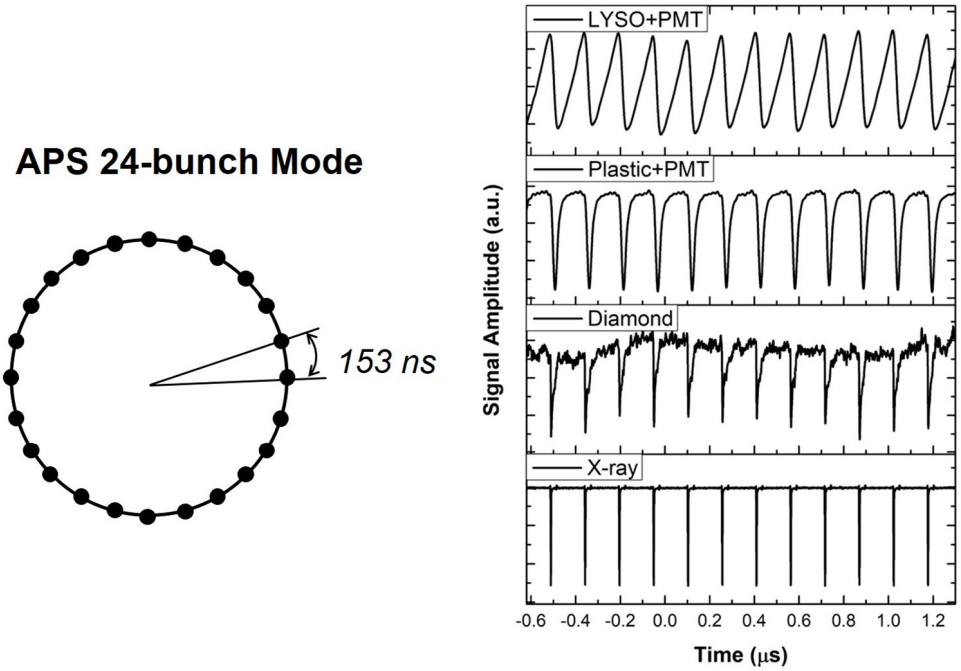

Fig. 4. Left: the APS storage ring configured in 24-bunch mode. Right: Detector responses to X-ray pulses, from top to bottom: LYSO and PMT detector pair, plastic and PMT detector pair, a quadrant of the diamond detector, and the beamline timing signal.

readout. Under continuous X-ray pulse illumination at the 24 bunch mode, correspond scintillator pulses were generated. However, due to the rapid drain of charge at the MCPs, the MCP-PMT was found non-responsive to the continuous scintillator and X-ray pulses. In order to provide the MCP-PMT with enough time to recharge, the MCP-PMT high voltage connection was reconfigured into a gated photocathode mode, as shown in Fig. 3. The MCPs and anode were biased with a constant negative high voltage HV_{MCPs}, while the bias voltage of photocathode was controlled by a gate unit consisting of a pulse generator and two power supplies. The two power supplies were set at different negative bias voltages, $HV_{Photocathode1}$ was higher than HV_{MCPs}, and $HV_{Photocathode2}$ was slightly lower than HV_{MCPs}. The pulse generator produced pulsed signals to switch the bias voltage of photocathode between these two power suppliers. $HV_{Photocathode1}$ applied a forward potential difference between photocathode and MCP surface, setting the gate operation "OFF" mode so that photoelectrons were accelerated towards the MCP for signal detection, while $HV_{Photocathode2}$ applied a reverse potential difference between photocathode and MCP surface, setting the gate operation "ON" mode, stopping the photoelectrons for avalanche emissions in MCP. The gate "ON" period allowed MCPs to recover from charge drain during gate "OFF" period. The MCP-PMT was placed at a 90° angle with respect to the X-ray beam direction to avoid direct interact of MCP-PMT with X-rays.

During all the measurement, a synchrotron timer provided by the APS beamline was used as the trigger signal. All data were recorded in waveform format using a Tektronix DPO 71254 4-channel 12.5 GHz 50 GS/s oscilloscope. The waveforms were analyzed offline with MATLAB based analysis code to extract the signal amplitude, rise time and decay time.

3. Results and discussion

3.1. 24-bunch mode experiment with dynode PMT, scintillator and diamond detectors

The proof of concept experiment was performed with a series of detectors during the standard 24-bunch mode of APS operation, illustrated by the diagram in the left panel of Fig. 4. In each circle, 102 mA

Table 1
Detector responses to X-ray pulses for the proof of concept experiment.

Detector	Rise time (ns)	Decay time (ns)
LYSO + PMT1	18.4 ± 0.6	80.7 ± 1.8
Plastic + PMT2	12.4 ± 0.2	26.7 ± 0.9
Diamond	2.0 ± 0.2	28.3 ± 6.2

Table 2
Diamond detector responses to X-ray pulse intensity.

X-ray intensity (photon/s)	Amplitude (mV)	Rise time (ns)	Decay time (ns)
5.0×10^{12}	3.9 ± 0.3	2.0 ± 0.2	19.9 ± 2.8
2.5×10^{12}	1.8 ± 0.1	2.0 ± 0.3	19.6 ± 4.7
1.0×10^{12}	1.5 ± 0.1	2.1 ± 0.3	17.5 ± 3.2
5.0×10^{11}	0.8 ± 0.2	1.8 ± 0.3	17.2 ± 6.7

current was filled in 24 singlets (single bunches) with a nominal current of 4.25 mA per bunch and a spacing of 153 nanoseconds between singlets [26]. The right panel of figure 4 shows the summarized detector responses to X-ray pulses, including LYSO and dynode PMT detector pair, plastic and dynode PMT detector pair, and a quadrant of the diamond detector, respectively. The beam timing signals were also recorded and plotted in the figure. All of the detectors showed sufficient response time to resolve individual X-ray pulses with ~153 ns spacing between pulses, demonstrated the concept of time-resolved X-ray measurement. The rise time and decay time of different detector configurations were extracted from the recorded data histograms and compared in Table 1.

The waveform shapes and timing responses results showed that LYSO exhibited a slower response to X-ray pulses than the plastic scintillator, and diamond exhibited the fastest rise time response. Here, the LYSO crystal and plastic scintillator showed much longer rise and decay times than reported data [27–29]. A later study revealed that the X-ray beam intensity was out of the scintillator and PMT dynamic range and the dynode PMTs were operated at a low bias voltage condition, resulting in slow responses to the X-ray induced scintillation light. Nevertheless, the clear distinction of individual X-ray pulses proved the capability of these fast scintillator and photodetector pairs for time-resolved X-ray measurement.

3.2. Intensity dependence with dynode PMT, scintillator and diamond detectors

The dependence of detector responses on X-ray intensity was also studied following the 24-bunch mode experiment. The signals from LYSO and plastic scintillators were saturated for the range of X-ray intensities. The diamond detector exhibited clear intensity dependence of its response to X-ray pulses, and the results were reported in Table 2. The amplitude of the diamond signal exhibits an expected linear relationship to the beam intensity. The rise and decay times of the diamond detector kept almost constants as expected during the intensity dependence measurement. Since the diamond detector is a semiconductor detector, the reverse of the signal polarity was also observed when we reversed the diamond bias voltage polarity.

3.3. Hybrid mode experiment with gated MCP-PMT and LYSO

The Argonne 6 × 6 cm^2 fast-timing MCP-PMT was gated during the time-resolved X-ray measurement, adjusting the photocathode "ON/OFF" periods could provide the MCP-PMT enough recovery time to compensate the drain of charge during large simultaneous electron avalanche emissions. We studied the MCP-PMT responses dependence on MCP bias voltage, slit size (beam intensity), and the gate "ON" time. The experiment on the coupled MCP-PMT and LYSO detector pair was performed during the special hybrid fill operating mode as illustrated in Fig. 5. A single bunch containing 16 mA is isolated from

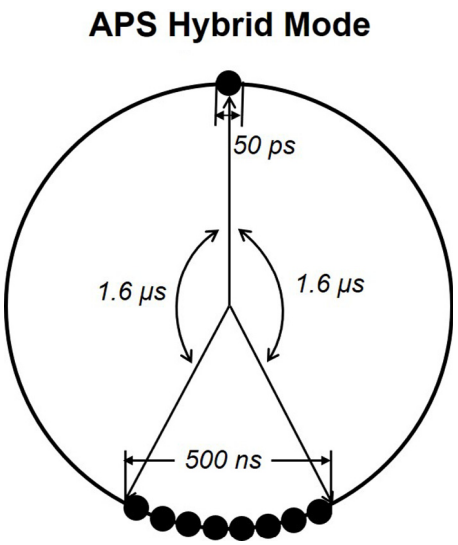

Fig. 5. Diagram illustration of APS hybrid fill operating mode.

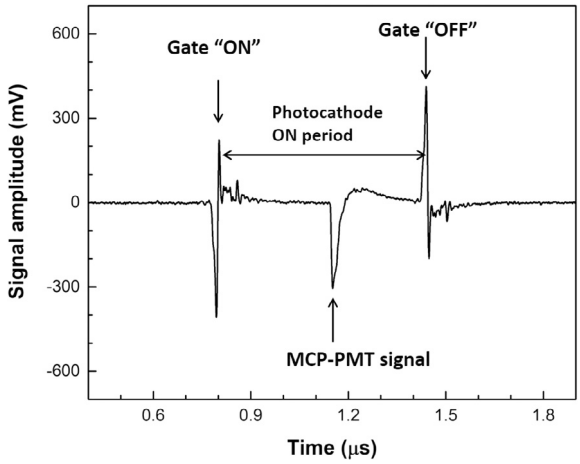

Fig. 6. Waveform of the gated MCP-PMT response to the main single X-ray bunch, the MCP-PMT was coupled with LYSO scintillator.

the remaining bunches by symmetrical 1.594 μs gaps. The remaining current is distributed in 8 groups of 7 consecutive bunches with a maximum of 11 mA per group, a periodicity of 68 ns, and a gap of 51 ns between groups, and the total length of the bunch train is 500 ns.

3.3.1. MCP bias voltage dependence

The MCP-PMT responses dependence on MCP bias voltage was performed by varying the entire MCP stack bias voltage. The photocathode "ON/OFF" voltages were adjusted accordingly so that the HV difference between the photocathode and the MCP surface was kept the same while the photocathode was "ON".

Fig. 6 shows a typical waveform of the gated MCP-PMT response to the main single X-ray bunch, the gate noise [30] induced by switching the gate "ON" and "OFF" was also captured by the oscilloscope. This gate noise can be reduced by applying a gate mesh to independently operating the reverse voltage to gate "OFF" the photocathode. The photocathode on period between the "ON" and "OFF" noise is ~620 ns, as set by the pulse generator. The MCP-PMT time responses were extracted and listed in Table 3. The mean LYSO decay time of 33 ns is shorter than the reported value of 43 ns [27]. This is due to the doping concentration difference between our LYSO sample and the one in the reference. The decay time of cerium doped LSO/LYSO crystals depends

Table 3
MCP-PMT and LYSO pair detector responses to X-ray pulse intensity.

HV MCP stack	Amplitude (mV)	Rise time (ns)	Decay time (ns)
2750 V	18 ± 4	6.2 ± 1.0	28.5 ± 11.2
2800 V	69 ± 13	6.1 ± 0.9	36.5 ± 8.5
2850 V	129 ± 21	6.0 ± 0.8	33.3 ± 8.1
2900 V	211 ± 34	5.8 ± 0.8	33.2 ± 6.4

Table 4
MCP-PMT and LYSO pair detector responses to X-ray beam intensity.

Slit size	Amplitude (mV)	Rise time (ns)	Decay time (ns)
100 μm	73 ± 13	4.9 ± 1.0	33.1 ± 8.3
200 μm	150 ± 21	5.2 ± 0.9	33.6 ± 6.4
300 μm	201 ± 34	5.3 ± 0.8	32.8 ± 5.3
500 μm	273 ± 45	5.2 ± 0.6	32.0 ± 4.5

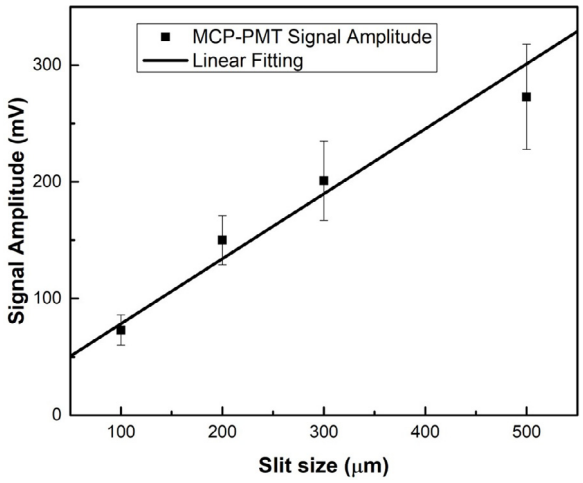

Fig. 7. MCP-PMT and LYSO pair detector signal amplitude dependent on the slit size (relative beam intensity).

on the ratio between different dopants [31], the faster decay time indicates a slightly higher doping concentration in our LYSO sample. The signal amplitude increases with the bias voltage of the MCP stack, attribute to the higher MCP gain at a higher bias voltage.

3.3.2. Beam intensity dependence

The MCP-PMT responses dependence on X-ray beam intensity was also measured and the results were reported in Table 4. Here, the slit sizes were recorded as an indication of the relative X-ray beam intensity. The MCP-PMT signal amplitude exhibited clearly linear dependence on the beam intensity variation as plotted in Fig. 7, indicating a sensitive response of the coupled MCP-PMT and LYSO detector pair to time-resolved X-ray pulses. The rise and decay times kept constants at different X-ray beam intensity conditions.

3.3.3. Gate "ON/OFF" time dependence

The above 500 ns photocathode on time window was set to only allow the detector response to the main single X-ray bunch. By extending the gate "ON/OFF" time window, it is expected to detect the entire APS fill pattern, the hybrid fill pattern for this measurement. Fig. 8 shows the signal waveform after the time window was extended to 4.5 μs. The 8 groups of bunches train, 1.594 μm apart from the main single X-ray bunch signal, was recorded and time-resolved individually. Since the scintillation light of LYSO is not fast enough, the 7 consecutive bunches in each group were not able to be time-resolved here using the coupled LYSO and MCP-PMT detector pair. However, we achieved a clear separation of the 7 consecutive bunches in each group by coupling ultra-fast BaF_2 scintillator and ultraviolet (UV) sensitive MCP-PMT detector; details were also reported in this proceeding [17]. With

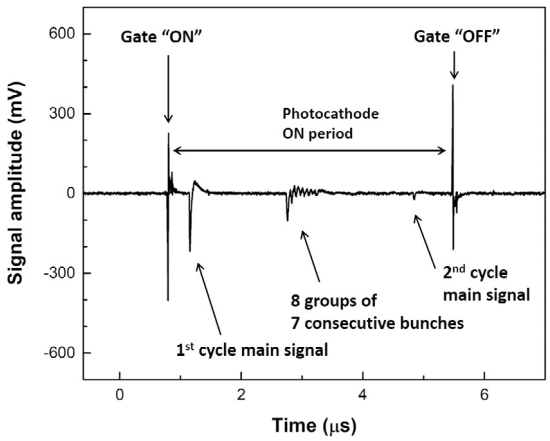

Fig. 8. MCP-PMT response waveform with operation time window extended over the full fill cycle time, the MCP-PMT was coupled with LYSO scintillator.

the time window extended longer than the APS fill circle time (3.6 μs), the main single X-ray bunch signal of a 2nd fill circle was observed as shown in Fig. 8. The amplitude of the 2nd fill circle signal was much lower than that of the 1st fill circle, indicating the MCP-PMT suffered from extensive charge drain, faster compensation of the charge drain is necessary for a longer time window operation.

4. Conclusions and outlook

In summary, we reported the first experimental demonstration of time-resolved X-ray measurements using APS 10-ID-B beamline. A series of X-ray detectors, including several coupled scintillator and photodetector pairs (plastic scintillator, high-Z LYSO crystal, dynode PMTs and fast-timing MC-PMT) and a diamond semiconductor detector were tested using the 24-bunch mode. The experiment shows promising results, providing a number of choices for time-resolved high-energy X-ray beam measurement. The fast X-ray pulse signals were observed for the first time from the next-generation fast-timing MCP-PMT by coupling it with LYSO scintillator and gating the photocathode; this provides promising results for its application towards ultrafast X-ray measurement.

Recent rapid development has shown great progress on high timing resolution X-ray imaging through direct detection approach. CdTe-based Advapix-Timepix3 detector [32] with 256 × 256 pixel matrix and 55 μm pixel pitch exhibits subpixel resolution while it was scanned with a 5 μm × 5 μm X-ray beam at energies of 24, 35, 70 and 120 keV respectively. The advantage of indirect detection approach using crystal scintillator and MCP-PMT is its acceptance and dynamic range. Ultrafast BaF_2 and MCP-PMT as an indirect approach provides total absorption, so 100% X-ray photons are accepted with a maximum dynamic range similar to calorimetry in particle detections. Further development of next-generation fast-timing MCP-PMT could focus on the following aspects to realize its application in X-ray imaging: (1) lower resistance ALD coated MCP for faster charge recovery. The current MCP-PMT contains MCP pairs with a resistivity of ~40 MΩ, this high resistivity requires a relatively long time for the MCP-PMT recharging. MCP with smaller resistivity of 3–5 MΩ should still be sufficient for secondary emission process, but it should dramatically improve the counting capability of the MCP-PMT. (2) solar blind (only sensitive to UV/VUV wavelength) photocathode for ultrafast BaF_2 scintillator crystal coupling. BaF_2 is presently the fastest known scintillator, it has two decay components in the scintillation light output. The fast scintillation light is emitted in bands centered at 220 and 195 nm with a decay constant of around 600 ps, and the slow component is emitted in bands centered at 310 nn with a decay constant of around 600 ns. The

current dynode-PMT and MCP-PMT we used are with glass window, has a typical detection range of 280 nm to 650 nm, not suitable to be coupled with BaF_2. A solar blind photocathode [33] coated on fused silica window should response only to the fast scintillation light from BaF_2, eliminating the slow component for picosecond fast-timing measurement. (3) pixelized readout for possible X-ray imaging. In the proof of concept experiment, we focused on the results of temporal resolution as the dynode PMT and MCP-PMT are not pixelized. Pixelized electronics readout such as the one implemented in Photek MAPMTs [34] and cross strip (XS) anode concept [35] should provide our MCP-PMT fine pixels for possible imaging application.

Acknowledgments

The authors would like to thank staffs at APS 10-ID-B for their beamline support. This research used resources of the Advanced Photon Source, a U.S. Department of Energy (DOE) Office of Science User Facility operated for the DOE Office of Science by Argonne National Laboratory, USA under Contract No. DE-AC02-06CH11357. Work at Argonne National Laboratory was supported by the U.S. Department of Energy, Office of Science, Office of High Energy Physics under contract No. DE-AC02-06CH11357. Work at Los Alamos National Laboratory was funded by U.S. Department of Energy, National Nuclear Security Administration through the C2 program.

References

[1] A. Momose, W. Yashiro, H. Maikusa, Y. Takeda, High-speed X-ray phase imaging and X-ray phase tomography with talbot interferometer and white synchrotron radiation, Opt. Express 17 (2009) 12540, http://dx.doi.org/10.1364/OE.17.012540.

[2] J.R. Royer, E.I. Corwin, A. Flior, M. Cordero, M.L. Rivers, P.J. Eng, H.M. Jaeger, Formation of granular jets observed by high-speed X-ray radiography, Nat. Phys. 1 (2005) 164, http://dx.doi.org/10.1038/nphys175.

[3] P. Cloetens, R. Barrett, J. Baruchel, J.P. Guigay, M. Schlenker, Journal of physics D: Applied physics phase objects in synchrotron radiation hard x-ray imaging, J. Phys. D: Appl. Phys. 29 (1996) 133, http://dx.doi.org/10.1088/0022-3727/29/1/023.

[4] K. Jorabchi, K. Kahen, C. Gray, A. Montaser, In situ visualization and characterization of aerosol droplets in an inductively coupled plasma, Anal. Chem. 77 (2005) 1253, http://dx.doi.org/10.1021/ac048576k.

[5] C. Crua, M.R. Heikal, M.R. Gold, Microscopic imaging of the initial stage of diesel spray formation, Fuel 157 (2015) 140, http://dx.doi.org/10.1016/j.fuel.2015.04.041.

[6] C. Rischel, A. Rousse, I. Uschmann, P. Albouy, J. Geindre, P. Audebert, J. Gauthier, E. Fröster, J. Martin, A. Antonetti, Femtosecond time-resolved X-ray diffraction from laser-heated organic films, Nature 390 (1997) 490, http://dx.doi.org/10.1038/37317.

[7] N. Parab, C. Zhao, R. Cunningham, L. Escano, K. Fezzaa, W. Everhart, A. Rollett, L. Chen, T. Sun, Ultrafast X-ray imaging of laser metal additive manufacturing processes, J. Synchrotron Radiat. 25 (2018) 1467, http://dx.doi.org/10.1107/S1600577518009554.

[8] Q. Guo, C. Zhao, L. Escano, Z. Young, L. Xiong, K. Fezzaa, W. Everhart, T. Sun, L. Chen, Transient dynamics of powder spattering in laser powder bed fusion additive manufacturing process revealed by in-situ high-speed high-energy x-ray imaging, Acta Mater. 151 (2018) 169, http://dx.doi.org/10.1016/j.actamat.2018.03.036.

[9] E. Reich, Ultimate upgrade for US synchrotron, Nature 501 (2013) 148–149, http://dx.doi.org/10.1038/501148a.

[10] C.W. Barnes, J. Fernandez, T. Hartsfield, R. Sandberg, R. Sheffield, J.P. Tapia, Z. Wang, Technology risk mitigation research and development for the matter-radiation interactions in extremes (MaRIE) project, AIP Conf. Proc. 1979 (2018) 160003, http://dx.doi.org/10.1063/1.5045002.

[11] Z. Wang, C.L. Morris, J.S. Kapustinsky, K. Kwiatkowski, S.L. Luo, Towards hard x-ray imaging at GHz frame rate, Rev. Sci. Instrum. 83 (2012) 10E510, http://dx.doi.org/10.1063/1.4731748.

[12] Z. Wang, On the single-photon-counting (SPC) modes of imaging using an XFEL source, J. Instrum. 10 (2015) C12013, http://dx.doi.org/10.1088/1748-0221/10/12/C12013.

[13] C. Hu, L. Zhang, R.-Y. Zhu, A. Chen, Z. Wang, L. Ying, Z. Yu, Ultrafast inorganic scintillators for gigahertz hard X-ray imaging, IEEE Trans. Nucl. Sci. 65 (2018) 2097, http://dx.doi.org/10.1109/TNS.2018.2808103.

[14] Ultrafast and high-energy X-ray imaging technologies and applications, MaRIE Summer 2016 workshop series, August, 2016, 2–3, Santa Fe, New Mexico.

[15] W. Lehmann, Edge emission of n-type conducting ZnO and CdS, Solid-State Electron. 9 (1966) 1107–1110, http://dx.doi.org/10.1016/0038-1101(66)90134-1.

[16] S.E. Derenzo, M.J. Weber, M.K. Klintenberg, Temperature dependence of the fast near-band-edge scintillation from CuI HgI 2 PbI 2 ZnO:Ga and CdS:In, Nucl. Instrum. Methods Phys. Res. A 486 (2002) 214–219, http://dx.doi.org/10.1016/S0168-9002(02)00705-2.

[17] L. Zhang, R. Zhu, et al., Ultrafast Inorganic Scintillator-Based Front Imager for Gigahertz Hard X-ray Imaging this proceeding.

[18] K.K. Hamamatsu Photonics, Photomultiplier Tubes: Basics and Applications, third ed., 2006.

[19] M. Akatsu, et al., MCP-PMT timing property for single photons, Nucl. Instrum. Methods Phys. Res. A 528 (2004) 763–775, http://dx.doi.org/10.1016/j.nima.2004.04.207.

[20] M. Minot, et al., Pilot production & commercialization of LAPPD™, Nucl. Instrum. Methods Phys. Res. A 787 (2015) 78–84, http://dx.doi.org/10.1016/j.nima.2014.11.025.

[21] J. Xie, et al., Design and fabrication of prototype 6 cm × 6 cm microchannel plate photodetector with bialkali photocathode for fast timing applications, Nucl. Instrum. Methods Phys. Res. A 784 (2015) 242, http://dx.doi.org/10.1016/j.nima.2014.10.050.

[22] J. Wang, et al., Design improvement and bias voltage optimization of glass-body microchannel plate picosecond photodetector, IEEE Trans. Nucl. Sci. 64 (2016) 1871–1879, http://dx.doi.org/10.1109/TNS.2016.2632748.

[23] J. Wang, et al., Development and testing of cost-effective, 6 cm × 6 cm MCP-based photodetectors for fast timing applications, Nucl. Instrum. Methods Phys. Res. A 804 (2015) 84, http://dx.doi.org/10.1016/j.nima.2015.09.020.

[24] C. Segre, et al., The MRCAT insertion device beamline at the advanced photon source, AIP Conf. Proc. 521 (2001) 419, http://dx.doi.org/10.1063/1.1291825.

[25] T. Zhou, W. Ding, M. Gaowei, G. Geronimo, J. Bohon, J. Smedley, E. Muller, Pixelated transmission-mode diamond X-ray detector, J. Synchrotron Radiat. 22 (2015) 1396–1402, http://dx.doi.org/10.1107/S1600577515014824.

[26] L. Emery, Recent operational data on continuous top-up operation at the advanced photon source, in: Proceedings of the 2001 Particle Accelerator Conference, vol. 4, 2001, p. 2599, http://dx.doi.org/10.1109/PAC.2001.987844.

[27] S. Seifert, J. Steenbergen, H. Dam, D. Schaart, Accurate measurement of the rise and decay times of fast scintillators with solid state photon counters, J. Instrum. 7 (2012) 9004, http://dx.doi.org/10.1088/1748-0221/7/09/P09004.

[28] S. Derenzo, W. Choong, W. Moses, Fundamental limits of scintillation detector timing precision, Phys. Med. Biol. 59 (2014) 3261–3286, http://dx.doi.org/10.1088/0031-9155/59/13/3261.

[29] R. Hoischen, et al., Fast timing with plastic scintillators for in-beam heavy-ion spectroscopy, Nucl. Instrum. Methods Phys. Res. A 654 (2011) 354–360, http://dx.doi.org/10.1016/j.nima.2011.07.013.

[30] A. Etile, D. Denis-Petit, L. Gaudefroy, V. Meot, O. Roig, A gated $LaBr_3$ (Ce) detector for border protection applications, Nucl. Instrum. Methods Phys. Res. A 877 (2018) 323–327, http://dx.doi.org/10.1016/j.nima.2017.08.053.

[31] T. Szczesniak, M. Moszynski, A. Syntfeld-Kazuch, L. Swiderski, M.A. Spurrier Koschan, C.L. Melcher, Timing resolution and decay time of LSO crystals Co-Doped with calcium, IEEE Trans. Nucl. Sci. 57 (2010) 1329–1334, http://dx.doi.org/10.1109/TNS.2009.2035620.

[32] Mohamad Khalil, Erik.Schou Dreier, Jan Kehres, Jan Jakubek, Ulrik.Lund Olsen, Subpixel resolution in CdTe Timepix3 pixel detectors, J. Synchrotron Radiat. 25 (2018) 1650–1657, http://dx.doi.org/10.1107/S1600577518013838.

[33] Z.Y. Wei, R.Y. Zhu, H. Newman, Z.W. Yin, Light yield and surface treatment of barium fluoride crystals, Nucl. Instrum. Methods Phys. Res. A 61 (1991) 61–66, http://dx.doi.org/10.1016/0168-583X(91)95561-Q.

[34] James Milnes, Jon Lapington, Steve Leach, Performance of high pixel density multi-anode microchannel plate photomultiplier tubes, in: 2017 Nuclear Science Symposium and Medical Imaging Conference, Atlanta, GA, 2017.

[35] Oswald H.W. Siegmund, John V. Vallerga, Jason B. McPhate, Anton S. Tremsin, Next generation microchannel plate detector technologies for UV astronomy, in: Proc. SPIE, vol. 5488, UV and Gamma-Ray Space Telescope Systems, 2004, http://dx.doi.org/101117/12562696.